LETTER • OPEN ACCESS

Identification of symmetric and asymmetric responses in seasonal streamflow globally to ENSO phase

View the article online for updates and enhancements.

Related content

Recent citations

Environmental Research Letters

LETTER

Identification of symmetric and asymmetric responses in seasonal streamflow globally to ENSO phase

Donghoon Lee[1] , Philip J Ward[2] and Paul Block[1,3]

1   Department of Civil and Environmental Engineering, University of Wisconsin-Madison, Madison, WI, United States of America
2   Institute for Environmental Studies (IVM), VU University Amsterdam, De Boelelaan 1087, 1081 HV Amsterdam, The Netherlands
3   Author to whom any correspondence should be addressed.

E-mail: paul.block@wisc.edu

Abstract

The phase of the El Niño Southern Oscillation (ENSO) has large-ranging effects on streamflow and hydrologic conditions globally. While many studies have evaluated this relationship through correlation analysis between annual streamflow and ENSO indices, an assessment of potential asymmetric relationships between ENSO and streamflow is lacking. Here, we evaluate seasonal variations in streamflow by ENSO phase to identify asymmetric (AR) and symmetric (SR) spatial pattern responses globally and further corroborate with local precipitation and hydrological condition. The AR and SR patterns between seasonal precipitation and streamflow are identified at many locations for the first time. Our results identify strong SR patterns in particular regions including northwestern and southern US, northeastern and southeastern South America, northeastern and southern Africa, southwestern Europe, and central-south Russia. The seasonally lagged anomalous streamflow patterns are also identified and attributed to snowmelt, soil moisture, and/or cumulative hydrological processes across river basins. These findings may be useful in water resources management and natural hazards planning by better characterizing the propensity of flood or drought conditions by ENSO phase.

1. Introduction

Over the past decades, the El Niño Southern Oscillation (ENSO) has been classified as the most important determinant of variability in global precipitation [1–6]. Phases of ENSO (El Niño and La Niña) also strongly affect both average and extreme streamflow (river discharge) and hydrologic conditions (e.g. droughts and floods) globally [7–14].

From prior studies, relationships between fluctuations in global streamflow and ENSO indices have been evaluated using correlation and regression analyses [8–10, 12, 13]. These correlations and regressed tendencies between streamflow and past or concurrent ENSO phase (or indices) provide useful information about typical ENSO impacts on water resources, assuming a symmetric (linear) teleconnection between ENSO variability (e.g. high-flow in El Niño and low-flow in La Niña). This assumption of linearity is also a prevalent view of the global climatic response

associated with ENSO, particularly in tropical locations [15]. In some regions, however, the ENSO-climate relationships are asymmetric or non-linearly teleconnected between ENSO phases [16–18].

Despite the asymmetric (or nonlinear) ENSO-climate patterns studied globally [15, 16, 19–24], there has been relatively little attention paid to asymmetric ENSO-streamflow relationships. Khan *et al* [25] confirm a higher nonlinear dependence between ENSO and seasonal streamflow compared to classical linear dependence at multiple tropical rivers using mutual information that can statistically capture both linear and non-linear mutual dependence. Fleming and Dahlke [26] identify parabolic teleconnections between ENSO and annual streamflow of several large river basins globally using an Akaike Information Criterion-based polynomial selection. These nonlinear modeling approaches arguably better describe the ENSO-streamflow variation than conventional linear approaches, however these studies do not

fully explain the physical mechanisms associated with ENSO-induced climate patterns which may further improve understanding of responses in streamflow to each ENSO phase. This motivates the identification and physical explanation of anomalously asymmetric or symmetric responses in streamflow to ENSO phase globally.

This analysis is unique in comparison with recent studies of ENSO-climate responses, which often focus on annual (hydrological year) mean or maximum streamflow; here a global focus at the seasonal-scale is addressed given that ENSO can lead to seasonal shifts in weather patterns globally [6] and the seasonality of streamflow also varies significantly globally [8, 27]. Additionally, we evaluate and explain the potential for diverse responses between well-known ENSO-precipitation and ENSO-streamflow relationships, the later often exhibiting broad spatiality given the integration of cumulative hydrological processes across a river basin [10, 28, 8]. This improved understanding of ENSO-induced anomalous seasonal streamflow patterns can provide an indication of the likelihood of hydrological conditions (drought and flood) concurrently or from a season-ahead perspective [16], benefiting water resources management, particularly in regions with strong El Niño or La Niña-streamflow signals.

In this paper, we investigate composite mean tendencies of seasonal streamflow in each ENSO phase and identify asymmetric and symmetric ENSO-streamflow patterns using streamflow observations, simulations from a global hydrological model for regions having limited streamflow observations, and reanalyzed global precipitation and hydrologic conditions.

2. Data and methods

2.1. Data

For this study, streamflow observations are obtained from the Global Runoff Data Centre (GRDC) [29] and the US Geological Survey (USGS). From GRDC, we select stations with a minimum catchment area greater than $10\,000\,km^2$. All stations are verified as having *no* or *allowable* regulation on streamflow climatology and seasonality from upstream reservoirs and dams by digitally mapping all dams near selected stations from the Global Reservoir and Dam database (GranD) [30] and the HydroLAKES dataset [31] and subsequently inspecting year-to-year daily and monthly streamflow patterns at each station (see Lee *et al* [32] for full description of station selection procedure). From USGS, we use the Hydro-Climatic Data Network (HCDN) [33], which lists pre-validated natural streamflow stations, and select those with a minimum catchment area larger than $500\,km^2$. To retain stations with an adequate number of records in ENSO years, we select GRDC and

HCDN stations having at least 10 years in each ENSO phase (El Niño, La Niña, and Neutral). Thus in total, we select 761 streamflow stations globally (534 GRDC + 227 HCDN) with a 77 year average record (figure S1).

We utilize $0.5° \times 0.5°$ gridded streamflow simulations over the period 1958–2000 (43 years) from Ward *et al* [34] to cover ungauged areas. Streamflow is generated using PCR-GLOBWB (PCRaster GLOBal Water Balance) [35, 36], which has been validated on long-term streamflow characteristics, terrestrial water storage, and extreme discharge values [37, 38, 34]. The PCR-GLOBWB model is forced with daily meteorological data from the WATCH (Water and Global Change) project [39]. The WATCH forcing data 20th Century (WFD) was initially derived from the ERA-40 reanalysis product [40] and were subjected to corrections based on elevation, precipitation gauges, and time adjustments to reflect monthly observations from daily values [39].

Precipitation reanalysis data ($0.5° \times 0.5°$ resolution) during the same model period (1958–2000) are adopted from WFD (www.eu-watch.org/data_availability) for land surface areas and ERA40 (http://apps.ecmwf.int/datasets/data/era40-daily) for ocean areas. For ERA40 precipitation, the convective and large-scale precipitation fields are summed to produce total precipitation.

In order to evaluate dry/wet (or drought/flood) conditions of ENSO-streamflow patterns, the global self-calibrating Palmer Drought Severity Index (scPDSI) ($0.5° \times 0.5°$ resolution) for the same model period is adopted from (https://crudata.uea.ac.uk/cru/data/drought/) [41]. The scPDSI defines relative soil moisture conditions from −4 (extremely dry) to +4 (extremely wet) using a water-budget system of soil characteristics and historical records of precipitation and potential evaporation.

ENSO years are classified by the Center for Ocean-Atmospheric Prediction Studies (COAPS) starting in 1869 based on observed sea-surface temperature (SST) anomalies over the tropical Pacific Ocean (4° S–4° N, 150° W–90° W). Full details of classification are available on the COAPS website (http://coaps.fsu.edu/jma). Our model simulation period includes ten El Niño events (1963–64, 1965–66, 1969–70, 1972–73, 1976–77, 1982–83, 1986–87, 1987–88, 1991–92, and 1997–98) and ten La Niña events (1964–65, 1967–68, 1970–71, 1971–72, 1973–74, 1974–75, 1975–76, 1988–89, 1998–99, and 1999–00). These events are used to create ENSO phase composites for the gridded streamflow simulations, precipitation reanalysis data, and scPDSI, while for streamflow observations, all corresponding COAPS ENSO years are used. The seasonal spatial patterns of SST anomalies for ten El Niño and ten La Niña years are illustrated with the ENSO index in the supplementary data (figures S2 and S3 available at stacks.iop.org/ERL/13/044031/mmedia).

We define four seasons per year to classify ENSO periods: September–November (SON) and December–February (DJF) for ENSO developing-mature periods and Mar-May (MAM) and June–August (JJA) for ENSO mature-decaying periods.

2.2. Methods

A lognormal distribution is used to fit seasonal streamflow globally, having been demonstrated to be an appropriate distribution for positively skewed and non-negative hydrometeorological variables (e.g. annual or seasonal streamflow) [42]. Here, all seasonal streamflow records in each ENSO phase (each 10 years for model simulations) and for climatology (all 43 years for model simulations) are separately fit to a log-normal distribution.

To evaluate potential differences between ENSO phase and climatological log-normal distributions of seasonal streamflow, we compare average standard anomalies of logarithms. The average anomaly z_{ENSO} for each ENSO phase ($n = 10$ for model simulations) is calculated as

$$z_{ENSO} = \frac{1}{n} \sum_{i=1}^{n} \frac{x_i - \mu_x}{\sigma_x} \qquad (1)$$

where x_i is the logarithm of seasonal streamflow in ENSO phase year, and μ_x and σ_x are the climatological mean and standard deviation of logarithm of seasonal streamflow, respectively. From a normal table, z_{ENSO} values greater than 0.43 indicate an above-normal (AN) category in which the averaged anomaly falls into the top 33% of the climatological distribution (upper tercile), whereas values less than −0.43 imply a below-normal (BN) category and fall into the bottom 33% of the climatological distribution (lower tercile). z_{ENSO} values between the upper and lower tercile thresholds are classified as near-normal (NN). For the average anomaly of seasonal precipitation, we use unscaled values rather than logarithms in equation (1), assuming a Gaussian distribution. Normality of log-transformed seasonal streamflow and unscaled seasonal precipitation is assessed and identified in a fairly high percentage of stations and areas using the Lilliefors test ($\alpha = 0.05$) (figure S4). Since the scPDSI value is already conditioned to dry and wet conditions from −4 to 4, we use an average of scPDSI values in each ENSO phase rather than the anomaly. Also, scPDSI values lower than −1 (slightly-extremely dry) and higher than +1 (slightly-extremely wet) are considered as BN and AN categories, respectively.

The statistical significance of the averaged anomaly is assessed using a bootstrap test [43]. The empirical distribution of z_{ENSO} is estimated by resampling z_{ENSO} values with randomly selected n seasonal streamflow and precipitation 10 000 times. The confidence intervals ($\alpha = 0.10$) are estimated by the percentile method [43], such that z_{ENSO} values smaller (larger) than the 5*th* (95*th*) percentile of the bootstrap estimates are

considered statistically significant. z_{ENSO} values falling between the 5*th* and 95*th* percentiles are not statistically significant and classified into the NN category. The same approach is also applied to the averages of scPDSI rather than averaged anomalies. No field significance tests (e.g. Monte Carlo methods [44]) are applied to estimate spatial extents of ENSO signals, given the emphasis on identification of locally significant ENSO signals [16].
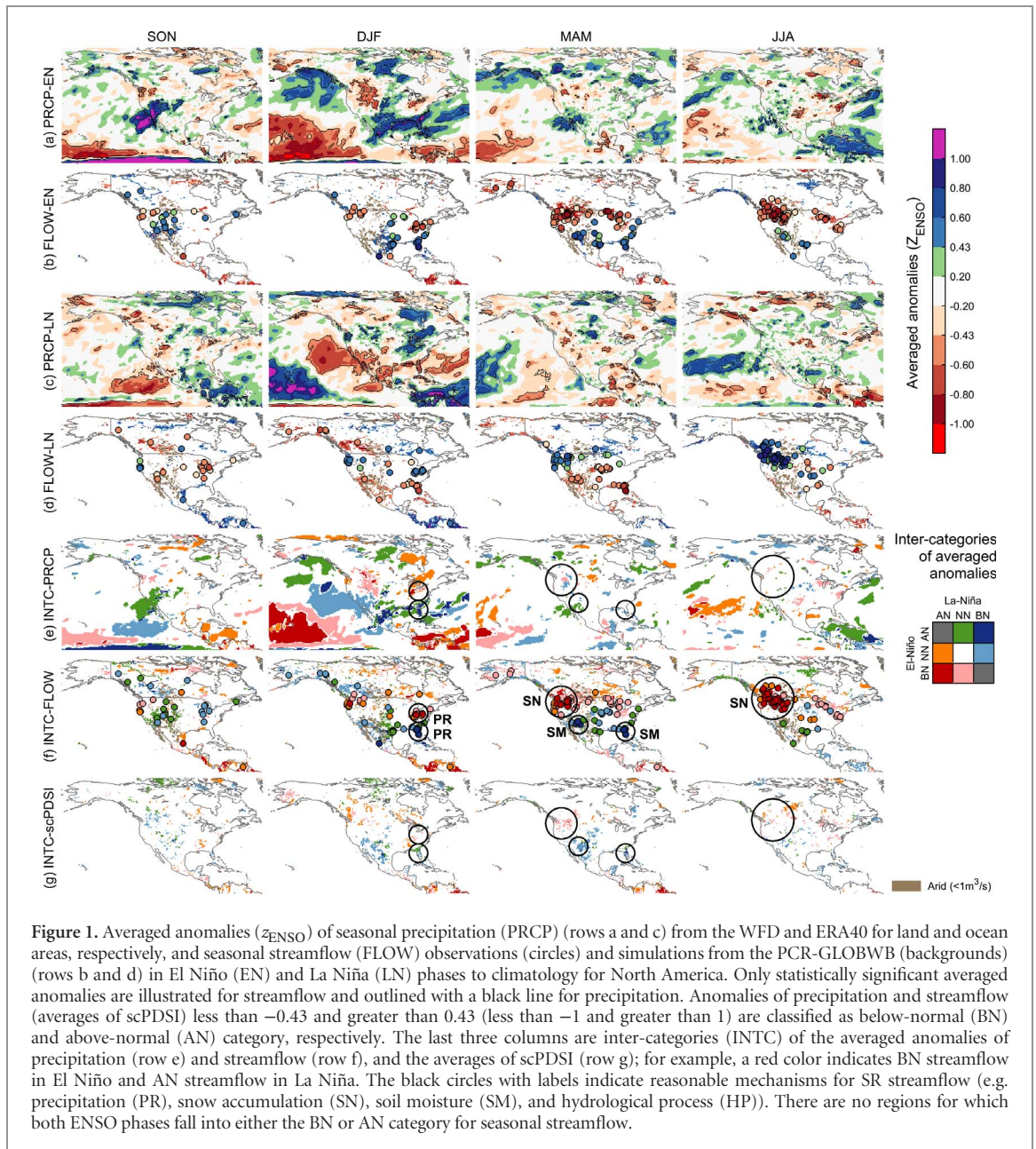
To understand the propensity for symmetric or asymmetric ENSO phase-streamflow and precipitation relationships at a given location, we categorize tercile-based averaged anomalies for each ENSO phase to form a 3×3 matrix (e.g. *Inter-categories of averaged anomalies* in figure 1). This is also applied to the averages of scPDSI with predefined thresholds (−1 and +1) for categorizing below and above-normal conditions. For a specific location, if the z_{ENSO} values for the two ENSO phases are separated by two categories (e.g. AN for El Niño and BN for La Niña), the local relationship is defined as a symmetric response (SR). If the z_{ENSO} values for the two ENSO phases are separated by a single category (e.g. AN and NN or BN and NN), this is defined as an asymmetric response (AR). The AR and SR relationship is assessed when at least one ENSO phase falls into the AN or BN category. The SR patterns of NN-NN cases are not investigated in this study. Also, reasonable mechanisms for SR streamflow patterns are highlighted (e.g. precipitation, snow accumulation or snowmelt, soil moisture, and hydrological process).

3. Results

Following the classification of seasonal variations in anomalous precipitation and streamflow by ENSO phase and AR or SR pattern, results are illustrated and described by continent (figures 1–5).

3.1. North America

For the El Niño phase in North America (figure 1), AN precipitation develops from the west coast of the US (e.g. the Great Basin) in SON due to increased storminess from the southeastern shift of cyclone activity [45, 46], which also leads to AN streamflow (figures 1(*a*) and (*b*), SON). In the south-central and southeast US, the extended Pacific jet stream and amplified storm tracks develop AN precipitation and streamflow in DJF [45], and AN streamflow persists until MAM (figures 1(*a*) and (*b*), DJF–MAM). Comparatively, in the La Niña phase, the Pacific jet stream reaches the continent in northwestern US and southwestern Canada in winter due to the increased blocking activity over the high latitudes of the eastern North Pacific [47], carrying AN precipitation and streamflow over northwestern and northeastern US in DJF, and BN precipitation and streamflow in the southern states of the US until MAM due to the
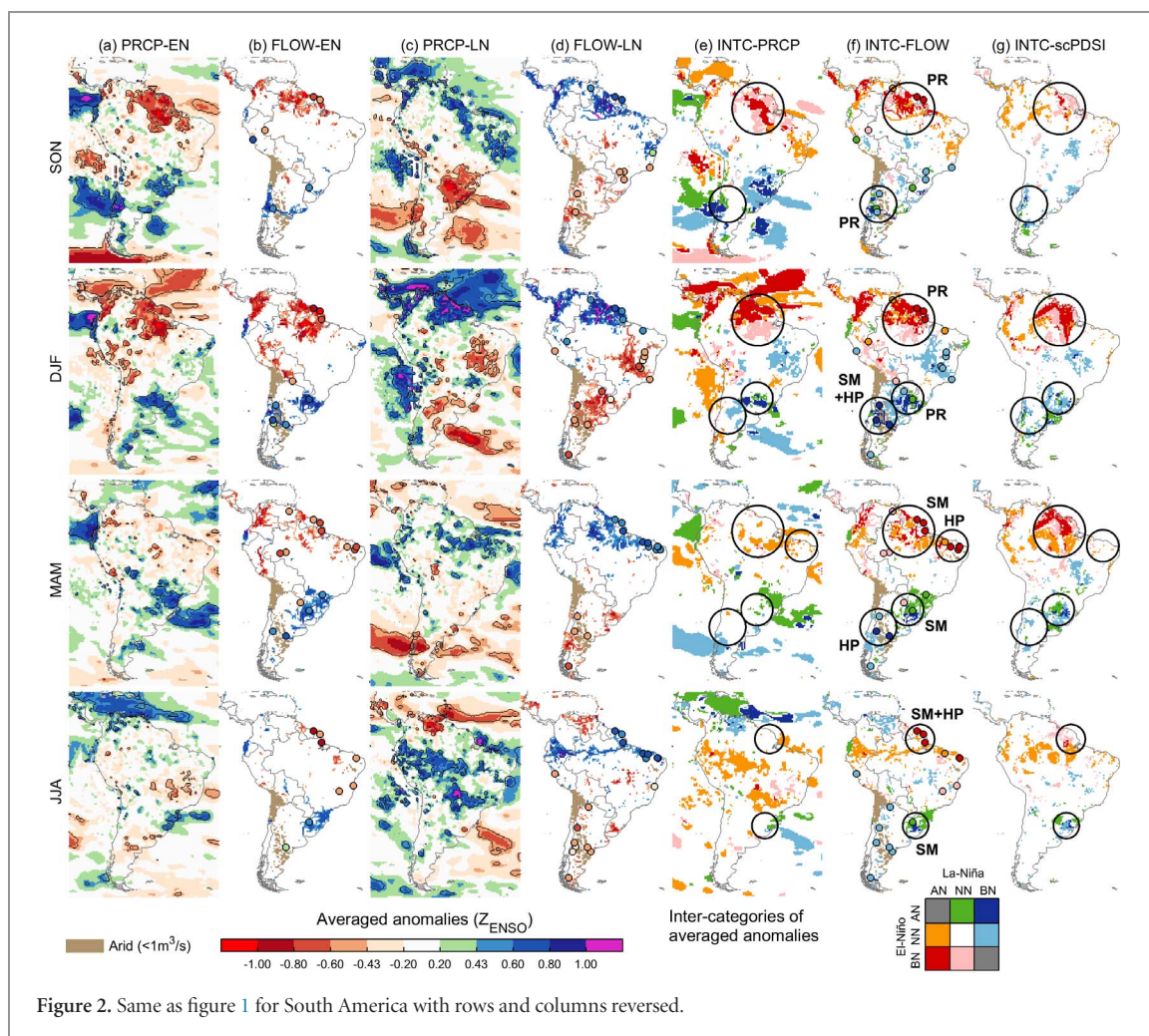
Figure 1. Averaged anomalies (z_{ENSO}) of seasonal precipitation (PRCP) (rows a and c) from the WFD and ERA40 for land and ocean areas, respectively, and seasonal streamflow (FLOW) observations (circles) and simulations from the PCR-GLOBWB (backgrounds) (rows b and d) in El Niño (EN) and La Niña (LN) phases to climatology for North America. Only statistically significant averaged anomalies are illustrated for streamflow and outlined with a black line for precipitation. Anomalies of precipitation and streamflow (averages of scPDSI) less than −0.43 and greater than 0.43 (less than −1 and greater than 1) are classified as below-normal (BN) and above-normal (AN) category, respectively. The last three columns are inter-categories (INTC) of the averaged anomalies of precipitation (row e) and streamflow (row f), and the averages of scPDSI (row g); for example, a red color indicates BN streamflow in El Niño and AN streamflow in La Niña. The black circles with labels indicate reasonable mechanisms for SR streamflow (e.g. precipitation (PR), snow accumulation (SN), soil moisture (SM), and hydrological process (HP)). There are no regions for which both ENSO phases fall into either the BN or AN category for seasonal streamflow.

deficient moisture transport from the tropical Pacific (figures 1(*c*) and (*d*), DJF–MAM).

Generally, precipitation and streamflow present similar anomalous patterns from season to season, however, dissimilar patterns are also evident. For example, compared to no or less significant ENSO-precipitation relationships in northwestern US and southwestern Canada in MAM, strong BN (AN) anomalies of streamflow develop and extend until JJA in the El Niño (La Niña) phase (figures 1(*a*)–(*d*), MAM–JJA). This SR pattern over the western US is consistent with the results of Kahya and Dracup [46], Cayan *et al* [48], and Dettinger *et al* [49]; Kahya and Dracup [46] also confirm that the driest El Niño-induced streamflow patterns occur during May–August over these regions. The reason for the distinctly different ENSO-association between streamflow and precipitation over these northern highland areas

during MAM–JJA is the influence of less (more) precipitation and warm (cold) temperatures impacting snow accumulation in the El Niño (La Niña) phase during fall and winter, which controls snowmelt peak-flow in the following seasons [50, 51, 52].

The tercile-based averaged anomalies for each ENSO phase (3×3 matrix) of precipitation, streamflow, and scPDSI for North America (figures 1(*e*)–(*g*)) illustrate the SR streamflow patterns for BN streamflow during El Niño and AN streamflow during La Niña for northwestern US and southwestern Canada (MAM–JJA) due to snow accumulation fed by pre-season precipitation (SN labels in figure 1(*f*)) and northeastern US in DJF with anomalous precipitation (PR label in figure 1(*f*)). Also, while the inverse SR streamflow pattern in the southeastern US during DJF is highly affected by precipitation, the same SR streamflow in the southwestern and southeastern US

Figure 2. Same as figure 1 for South America with rows and columns reversed.

during MAM appears related to anomalous soil moisture conditions (SM labels in figures 1(*e*)–(*g*)). Notably, AR streamflow patterns also exist for many locations (e.g. the southwestern and eastern central-east US in SON) and also near locations of SR patterns where strongly anomalous streamflow (AN or BN) transitions to moderate streamflow (NN) in one ENSO phase (e.g. the southeastern (DJF) and northwestern (MAM) US) (figure 1(*f*)).
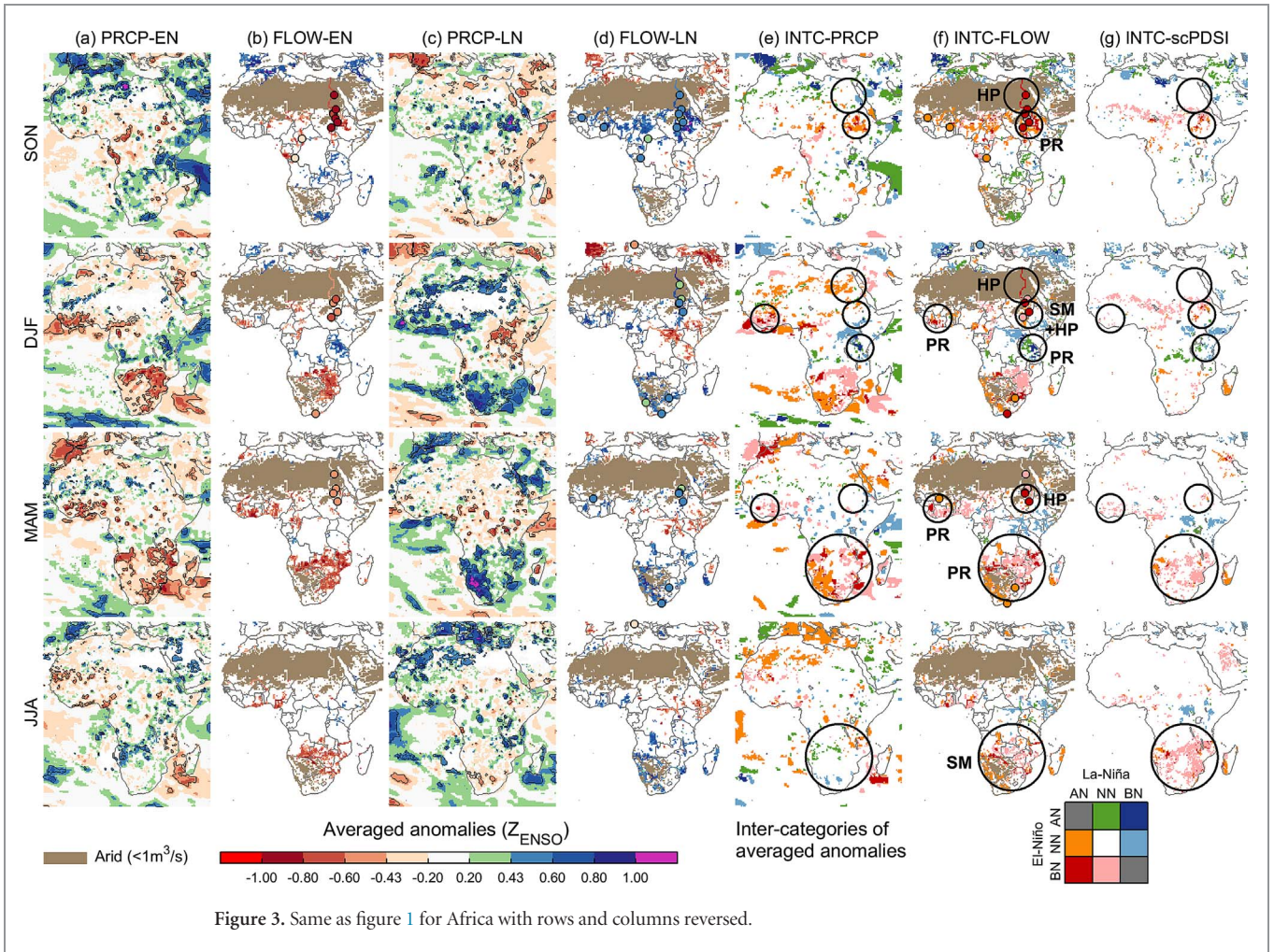
In North America, values in the inter-category of scPDSI are similar to those of precipitation, likely because of the dominant influence of precipitation in the scPDSI calculation (figures 1(*e*)–(*g*)). However, the aforementioned SR and AR streamflow patterns are classified into similar AR scPDSI patterns over northwestern, southeastern, and southwestern US in MAM where moderate precipitation (NN) exists, indicating the significant role of wetter and drier soil moisture conditions on AN and BN streamflow, respectively.

3.2. South America
In the El Niño phase, a strong shift toward BN precipitation develops in northeastern South America during SON and DJF, with greatly reduced streamflow ($z_{ENSO} < -1.00$) until MAM due to suppressed

rainfall by enhanced subsidence east of the El Niño-driven anomalous Walker circulation [1] (figures 2(*a*) and (*b*), SON-MAM). The opposite anomalous precipitation and streamflow patterns appear during La Niña, with patterns remaining until JJA (figures 2(*c*)–(*d*)). Specifically, the La Niña-induced strong AN precipitation and streamflow ($z_{ENSO} > 1.00$) occur in coastal regions (e.g. Venezuela and Guyana) (figures 2(*c*)–(*d*), DJF), which agrees with Ropelewski and Halpert [53]. The AN streamflow present in southeastern South America during the El Niño phase from DJF to JJA is a response of AN precipitation fed by warm moist air transported by a strengthening of the low-level jet and a weakening of the South Atlantic Convergence Zone [54]; conversely, BN precipitation and streamflow are present during DJF during the La Niña phase (figures 2(*c*)–(*d*)).

In South America, the AR and SR streamflow and scPDSI patterns are generally consistent with precipitation during ENSO developing-mature periods (SON–DJF), indicating the significant role of precipitation in developing AN and BN (also AR and SR) seasonal soil moisture and streamflow (figures 2(*e*)–(*g*)). For example, the strong SR precipitation and streamflow patterns appear in northeastern (SON–DJF) and southeastern (DJF) South America (PR
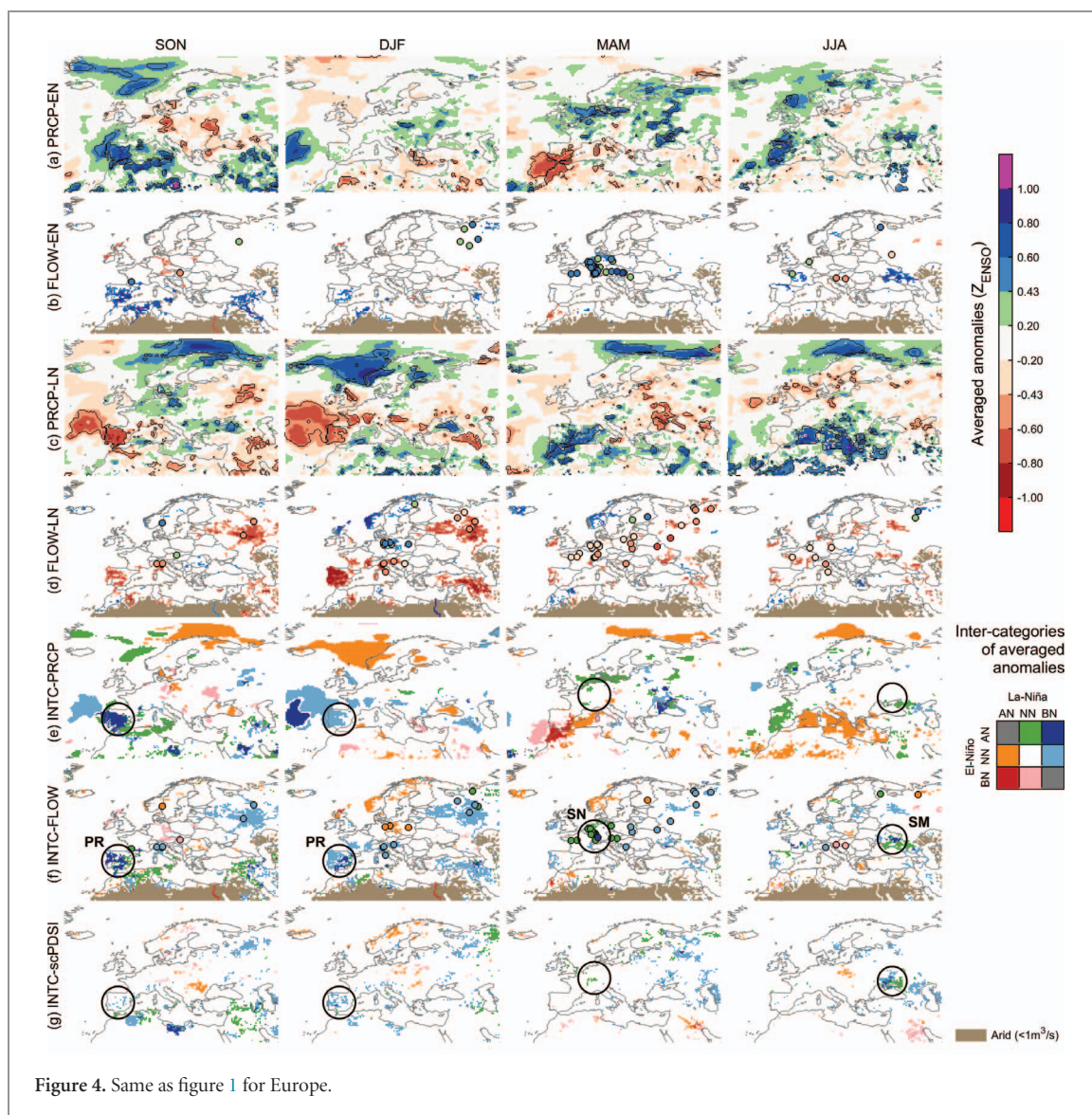
Figure 3. Same as figure 1 for Africa with rows and columns reversed.

labels in figures 2(*e*)–(*f*), SON–DJF). However, during ENSO mature-decaying periods (MAM–JJA), AR and SR streamflow are more related to anomalous soil moisture conditions than precipitation (figure 2(*e*)–(*g*), MAM–JJA). For example, SR streamflow is present in the southeastern and northeastern coastal regions where anomalous soil moisture controls streamflow (SM labels in figures 2(*e*)–(*g*), MAM–JJA). Also around this periods, SR streamflow is controlled by hydrological processes for some stations in southwestern and eastern South America, and occasionally exhibiting SR soil moisture conditions (HP or SM+HP labels in figures 2(*e*)–(*g*), DJF–JJA). AR streamflow patterns are present in the same vicinity (e.g. northeastern and southern South America in DJF) as well as locations in western (DJF) and southeastern (MAM–JJA) South America, having anomalous patterns in one ENSO phase.

3.3. Africa
Generally, west, central, and southern Africa tend to experience drier (wetter) precipitation and streamflow than normal across DJF–MAM during El Niño (La Niña) phases, excepting southern East Africa where the opposite patterns occur during SON–DJF (figures 3(*a*)–(*d*)). In southern Africa, these SR

patterns occur in spatially diverse areas; northeast southern Africa is affected in the El Niño phase and southwest southern Africa (the Kalahari Desert) in the La Niña phase (figures 3(*a*)–(*f*), DJF–MAM), which spatially matches with findings in Ropelewski and Halpert [53]. In contrast to moderate precipitation (NN) over south southern Africa during JJA in both ENSO phases, the anomalous streamflow signals continue from MAM, likely because of anomalously high soil moisture due to precipitation in MAM (figures 3(*a*)–(*d*) and (*g*), MAM–JJA).

Although less (or no) significant precipitation is present in northern East Africa (the Nile basin) during SON-MAM in the El Niño phase, which is also consistent with results from Mason and Goddard [16] and Sun *et al* [19], strong BN ($z_{ENSO} < -0.80$) streamflow occurs in downstream reaches of the Nile river in both observations (SON-MAM) and simulations (SON–DJF) (figures 3(*a*)–(*b*), SON-MAM). During the La Niña phase, streamflow is strongly AN ($z_{ENSO} > 1.00$) for SON-MAM, whereas AN precipitation is present only in upstream reaches of the Nile river in SON (figures 3(*c*)–(*d*), SON-MAM). This is the same ENSO-streamflow relationship found in Eltahir [55] and Dettinger and Diaz [8], and may result from integrating less significant but anomalous precipitation

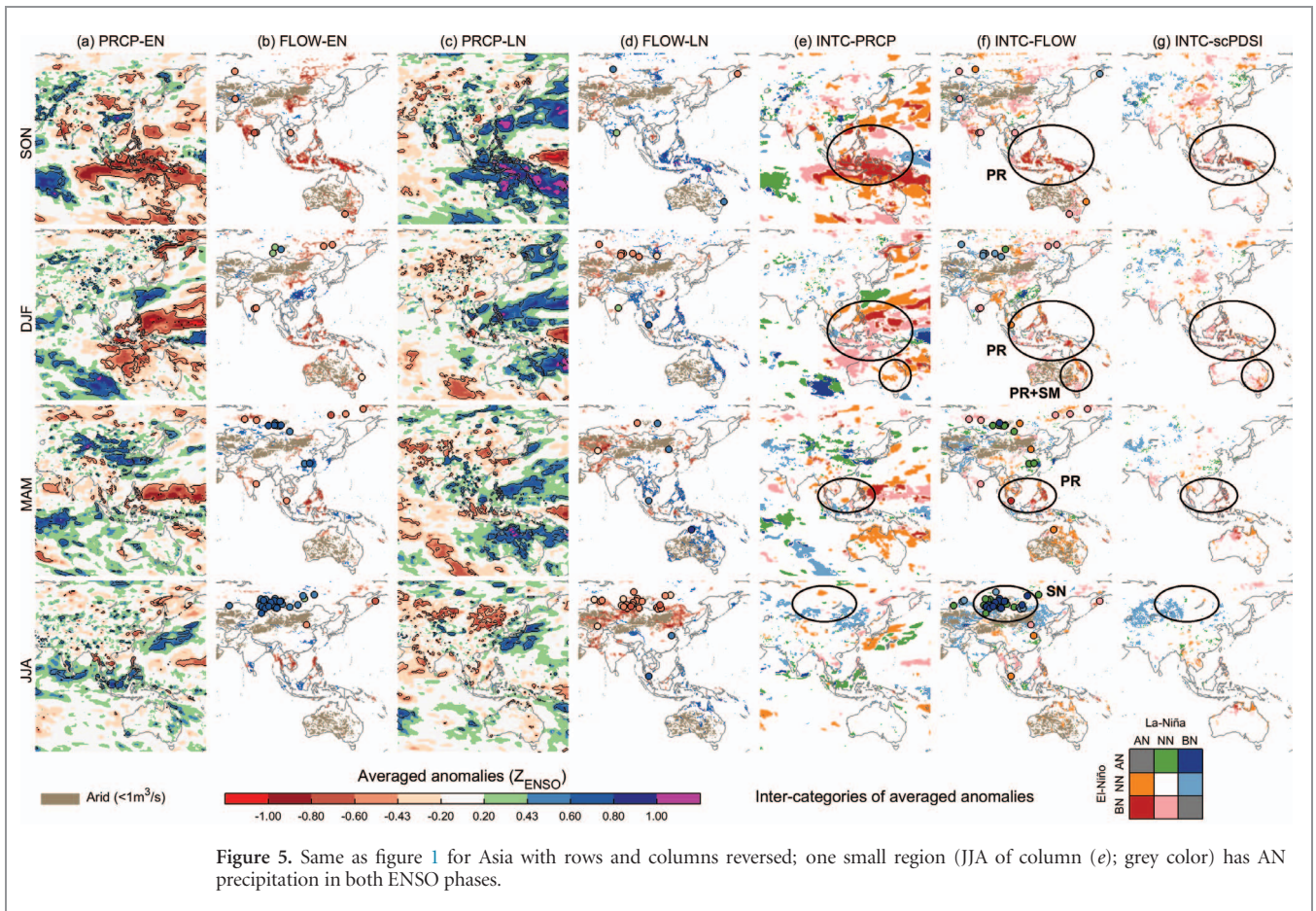**Figure 4.** Same as figure 1 for Europe.

from upstream reaches through hydrological processes (e.g. evapotranspiration, infiltration, and discharge) over large catchment areas [56, 57]. Additionally, in the upstream regions of the Nile river, anomalous soil moisture conditions affect the corresponding streamflow patterns more than precipitation in DJF (figures 3(e)–(g), DJF).

Likewise, anomalous streamflow patterns are generally consistent with the corresponding hydrological conditions (wetter or drier) from the scPDSI patterns, and the AR and SR streamflow patterns are similarly affected by precipitation (soil-moisture) during ENSO developing-mature (mature-decaying) periods (figures 3(e)–(g)). As noted, SR streamflow patterns are present in the Nile river (HP, PR, and SM+HP labels in figure 3(f), SON-MAM), parts of west Africa (PR labels in figure 3(f), DJF–MAM) southern Africa (PR and SM labels in figure figure 3(f), MAM–JJA), and southern east Africa (e.g. Tanzania) (PR label in figure 3(f), DJF). AR streamflow patterns, however, associated with drier to normal (wetter to normal) streamflow during El Niño (La Niña) appear in

west, central (Sahel), and southern Africa during most seasons, whereas the opposite AR streamflow pattern occurs in southern East Africa (figures 3(e)–(f)).

3.4. Europe

In Europe, AN (BN) precipitation and streamflow are expected in southwestern Europe (Spain, Portugal, and parts of the southwestern Mediterranean) in El Niño (La Niña) phases during SON (SON–DJF) due to strong (weak) anomalous cyclonic circulation over the western Mediterranean region delivering enhanced (diminished) moisture from the Atlantic Ocean during El Niño (La Niña) [58, 59] (figures 4(a)–(f), SON–DJF). The inverse SR precipitation pattern also appears in MAM over the same region, however, no (or less) distinct streamflow and soil moisture patterns are found in this case (figures 4(e)–(f), MAM). These opposing SR precipitation signals between fall (SON) and spring (MAM) are consistent with previous findings (e.g. Mariotti [58] and Shaman [60]).

Figure 5. Same as figure 1 for Asia with rows and columns reversed; one small region (JJA of column (*e*); grey color) has AN precipitation in both ENSO phases.

Expected BN precipitation and streamflow are also found in northeastern Europe (western Russia) and western Asia (Iran) in SON–DJF during La Niña (figures 4(*c*)–(*d*), SON–DJF). In central Europe (German, Poland, and Czech Republic), AN streamflow is present in the El Niño phase in MAM when snowmelt feeds spring peak-flow [61], whereas moderate BN spring streamflow appears in central and northeastern Europe (except Scandinavia) along with moderately drier precipitation during La Niña phases until JJA (figures 4(*a*)–(*d*), MAM–JJA).

Generally, the AR streamflow patterns associated with wetter to normal (drier to normal) streamflow in El Niño (La Niña) phases appear over much of the European continent (southwestern (SON–DJF), central (MAM), western Russia (SON-MAM), and western Asia (DJF and JJA)), except for the opposite AR streamflow patterns in parts of Scandinavia during DJF–MAM (figures 4(*e*)–(*f*)). Strong SR streamflow patterns appear in southwestern Europe (Spain and Portugal) during the fall and winter seasons (PR and HP labels in figure 4(*f*), SON–DJF) along with the same SR streamflow pattern across parts of central Europe (southern Germany) in MAM (SN label in figure 4(*f*), MAM). Although the SR streamflow pattern over southwestern Ukraine (JJA) is classified as SR hydrological conditions according to the scPDSI (SM label in figure 4(*f*), JJA), AR streamflow patterns are also present for the same AR

hydrological conditions in northwestern Europe (SON–JJA) (figures 4(*f*)–(*g*)).

3.5. Asia

During El Niños strong BN precipitation and streamflow develop in the tropical western Pacific (e.g. Indonesia, Philippines, and eastern Australia) during SON–DJF and South Asia (e.g. India) in SON, areas commonly affected by the modification of the Walker circulation [1] (figures 5(*a*)–(*b*), SON–DJF). Strongly AN precipitation and streamflow also appear in the tropical western Pacific during La Niña in SON–DJF, with AN precipitation and streamflow continuing through MAM over central and northeastern Australia due to increased active convection from the southwestward displacement of the South Pacific Convergence Zone [62, 2] (figures 5(*c*)–(*d*), SON-MAM).

In China during the El Niño phase, BN precipitation (SON) and streamflow (SON–DJF) are evident in the Yellow river basin, while AN precipitation and streamflow is expected in the Yangtze river basin in DJF–MAM, however the opposite patterns are not expected during the La Niña phase (figures 5(*a*)–(*d*), SON-MAM). This AR pattern is due to the asymmetry in anomalous circulation over the western North Pacific with strong (weak) anomalous anticyclonic activity during El Niño (La Niña) [63]. Compared

to moderate precipitation (NN) in North Asia in JJA during El Niño, BN precipitation is expected during La Niña followed by BN streamflow, particularly around northeastern and northwestern China, Mongolia, and southeastern Kazakhstan (figures 5(a)–(d), JJA). Central-south Russia, specifically the highland areas around Novosibirsk and Krasnoyarsk, presents distinct anomalous patterns in streamflow compared to precipitation during MAM–JJA in both ENSO phases (figures 5(a)–(d), MAM–JJA). This is also influenced by snow accumulation from precipitation and evapotranspiration in wintertime that feeds late-boreal spring to summer peak-flow [8, 27].

In Asia, SR streamflow is identified in the tropical western Pacific along with a strong SR precipitation pattern (PR labels in figures 5(e)–(f), SON-MAM), parts of eastern Australia (PR+SM label in figure 5(f), MAM), and central-south Russia (SN label in figure 5(f), JJA). The AR streamflow associated with drier to normal (wetter to normal) streamflow in El Niño (La Niña) phases appears in south Asia and China during SON-MAM, and the opposite AR streamflow pattern appears in northeastern and northwestern China, Mongolia, and southeastern Kazakhstan in JJA (figures 5(e)–(f)). Generally, these SR and AR streamflow patterns are fairly classified into the corresponding SR and AR hydrological conditions from the scPDSI patterns over most regions (figures 5(f)–(g)).

There is a small region where AN precipitation is evident for both phases of ENSO near southern Japan in JJA (gray colors in figure 5e, JJA), which is consistent with patterns and relationships found in Lu *et al* [64] and Chen *et al* [65]. Except in this region, there are no distinct regions for which both ENSO phases fall into either the BN or AN category for precipitation and streamflow globally.

4. Summary and discussion

In this study, we assess composite mean tendencies of seasonal streamflow based on observations and simulations from the PCR-GLOBWB model to identify AR and SR spatial patterns for ENSO phases. The analysis is performed equivalently on seasonal precipitation and scPDSI to evaluate local consistency with streamflow (figures 1–5).

The results illustrate variations of anomalous responses in streamflow from season to season globally, which extends past studies that correlate annual streamflow statistics with ENSO indices [9, 12, 13]. Globally, ENSO-induced anomalous streamflow are generally consistent with that of precipitation from season to season, indicating the significant role of precipitation in developing ENSO impacts on seasonal streamflow, however anomalous streamflow may also be present where no or less anomalous precipitation exists, typically expressed through lagged snowmelt impacts over highland areas (e.g. northwestern US, southwestern

Canada, central Europe, and central south Russia) and the integration of cumulative hydrological processes across river basins (e.g. the Nile river). While the intensification of anomalous precipitation during the ENSO developing-mature period is common in many locations globally, anomalous streamflow often extends in time through the mature-decaying period supported by soil moisture conditions bolstered by preseason precipitation (e.g. southwestern (the Great Basin) and southeastern US, northeastern (coastal regions), southwestern and southeastern South America, southern Africa, and southern East Africa).

AR and SR streamflow patterns are identified by classifying significant anomalies into tercile-based categories for each ENSO phase. This method yields rare SR streamflow patterns globally when only strong symmetric anomalies fall into AN and BN in each ENSO phase, for example in northeastern, southwestern, and southeastern (DJF–MAM) and northwestern (MAM–JJA) US, northeastern (SON-MAM), southwestern (SON-MAM), and southeastern (DJF–JJA) South America, northeastern (the Nile river) (SON-MAM) and southern (MAM–JJA) Africa, southwestern Europe (Spain and Portugal) (SON–DJF) and central Europe (southern Germany) (MAM), and tropical western Pacific (SON-MAM) and central-south Russia (JJA) (figures 1–5). Compared to SR streamflow patterns, AR streamflow patterns are broadly present globally where anomalous climate and streamflow patterns exist in only one ENSO-phase as well as locations where strongly anomalous streamflow often transitions to moderate. Generally, the identified AR and SR streamflow patterns closely resemble local scPDSI conditions, however, anomalous streamflow patterns are often more significant than the local soil moisture or precipitation conditions, perhaps due to the cumulative land processes throughout river basins.

This study is the first attempt to evaluate ENSO-induced anomalous seasonal streamflow and corresponding AR and SR streamflow patterns with complete (simulation) and extensive (observation) coverage of global land areas. Here we use typically-defined ENSO years to make composites, however ENSO diversity in amplitude, temporal evolution, and spatial pattern [66] uniquely affect streamflow anomalies and variability and may require additional investigation considering different ENSO types (e.g. Liang *et al* [67]). Also, further studies may be warranted to better understand lagged ENSO-climate signals on streamflow (e.g. snowpack) to quantify potential impacts.

The findings of this study may be useful in water resources management and natural hazards planning by better characterizing the seasonal propensity for flood or drought conditions and the associated AR and SR patterns per ENSO phase. This may be extended to aid in seasonal forecast development based on linear ENSO-streamflow relationships. For example, the identified AR and SR patterns may explain spatial

and temporal characteristics of the reported asymmetric annual flood risk (expected urban damage) between ENSO phases [68]. From this perspective, the findings of this study are valuable in regards to estimating the seasonal impacts of ENSO on global streamflow and for identifying regional teleconnections with ENSO and subsequent symmetric or asymmetric relationships.

Acknowledgments

ORCID iDs

Donghoon Lee https://orcid.org/0000-0001-5438-903X
Philip J Ward https://orcid.org/0000-0001-7702-7859
Paul Block https://orcid.org/0000-0003-1993-7496

References

[1] Ropelewski C F and Halpert M S 1987 *Mon. Weather Rev.* **115** 1606–26
[2] Ropelewski C F and Halpert M S 1989 *J. Clim.* **2** 268–84
[3] Bradley R S, Diaz H F, Kiladis G N and Eischeid J K 1987 *Nature* **327** 497–501
[4] Dai A, Fung I Y and Del Genio A D 1997 *J. Clim.* **10** 2943–62
[5] Dai A and Wigley T M L 2000 *Geophys. Res. Lett.* **27** 1283–6
[6] McPhaden M J, Zebiak S E and Glantz M H 2006 *Science (New York, NY)* **314** 1740–5
[7] Burn D H and Arnell N W 1993 *J. Hydrol.* **144** 381–404
[8] Dettinger M D and Diaz H F 2000 *J. Hydrometeorol.* **1** 289–310
[9] Dettinger M D, Cayan D R, Mccabe G J and Marengo J A 2000 Multiscale streamflow variability associated with El Niño/Southern Oscillation *El Niño and the Southern Oscillation: Multiscale Variability and Global and Regional Impacts* ed H F Diaz and V Markgraf (Cambridge: Cambridge University Press) pp 113–46
[10] Chiew F H S and McMahon T A 2002 *Hydrol. Sci. J.* **47** 505–522
[11] McCabe G J and Wolock D M 2008 *J. Hydrometeorol.* **9** 816–24
[12] Ward P J, Beets W, Bouwer L M, Aerts J C J H and Renssen H 2010 *Geophys. Res. Lett.* **37** 1–6
[13] Ward P J, Eisner S, Flörke M, Dettinger M D and Kummu M 2014 *Hydrol. Earth Syst. Sci.* **18** 47–66
[14] Ward P, Kummu M and Lall U 2016 *J. Hydrol.* **539** 358–78
[15] Hoerling M P, Kumar A and Zhong M 1997 *J. Clim.* **10** 1769–86
[16] Mason S J and Goddard L 2001 *Bull. Am. Meteorol. Soc.* **82** 619–38
[17] Jain S and Lall U 2000 *Water Resour. Res.* **36** 3641–51
[18] Lyon B and Barnston A G 2005 *J. Clim.* **18** 5095–109
[19] Sun X, Renard B, Thyer M, Westra S and Lang M 2015 *J. Hydrol.* **530** 51–65
[20] Okumura Y M, Sun T and Wu X 2017 *J. Clim.* **30** 4705–33
[21] Zhang T, Perlwitz J and Hoerling M P 2014 *Geophys. Res. Lett.* **41** 1019–25
[22] Hoerling M P, Kumar A and Xu T 2001 *J. Clim.* **14** 1277–93
[23] Wu A, Hsieh W W and Shabbar A 2005 *J. Clim.* **18** 1736–52
[24] Hsieh W W, Wu A and Shabbar A 2006 *Geophys. Res. Lett.* **33** L07714
[25] Khan S, Ganguly A R, Bandyopadhyay S, Saigal S, Erickson D J, Protopopescu V and Ostrouchov G 2006 *Geophys. Res. Lett.* **33** L24402
[26] Fleming S W and Dahlke H E 2014 *Environ. Res. Lett.* **9** 104007
[27] Lee D, Ward P and Block P 2015 *Hydrol. Earth Syst. Sci.* **19** 4689–705
[28] Probst J and Tardy Y 1987 *J. Hydrol.* **94** 289–311
[29] Global Runoff Data Centre 2007 *Major River Basins of the World / Global Runoff Data Centre* (Koblenz: Federal Institute of Hydrology (BfG): GRDC)
[30] Lehner B *et al* 2011 *Front. Ecol. Environ.* **9** 494–502
[31] Messager M L, Lehner B, Grill G, Nedeva I and Schmitt O 2016 *Nat. Commun.* **7** 13603
[32] Lee D, Ward P and Block P 2018 Attribution of large-scale climate patterns to seasonal peak-flow and prospects for prediction globally *Water Resour. Res.* **54**
[33] Lins H F 2012 USGS Hydro-Climatic Data Network 2009 (HCDN2009): US Geological Survey Fact Sheet 20123047 *Tech. rep.* USGS
[34] Ward P J, Jongman B, Weiland F S, Bouwman A, van Beek R, Bierkens M F P, Ligtvoet W and Winsemius H C 2013 *Environ. Res. Lett.* **8** 044019
[35] Van Beek L P H and Bierkens M F P 2009 The Global Hydrological Model PCR-GLOBWB: Conceptualization, Parameterization and Verification *Tech. Rep.* Utrecht University Utrecht
[36] Van Beek L P H, Wada Y and Bierkens M F P 2011 *Water Resour. Res.* **47** W07517
[37] Winsemius H C, Van Beek L P H, Jongman B, Ward P J and Bouwman A 2013 *Hydrol. Earth Syst. Sci.* **17** 1871–92
[38] Wada Y, van Beek L P H, Viviroli D, Dürr H H, Weingartner R and Bierkens M F P 2011 *Water Resour. Res.* **47** W07518
[39] Weedon G P, Gomes S, Viterbo P, Shuttleworth W J, Blyth E, Österle H, Adam J C, Bellouin N, Boucher O and Best M 2011 *J. Hydrometeorol.* **12** 823–48
[40] Uppala S M *et al* 2005 *Q. J. R. Meteorol. Soc.* **131** 2961–3012
[41] van der Schrier G, Barichivich J, Briffa K R and Jones P D 2013 *J. Geophys. Res. Atmos.* **118** 4025–48
[42] Stedinger J R 1980 *Water Resour. Res.* **16** 481–90
[43] Efron B and Tibshirani R J 1993 *An Introduction to the Bootstrap* (Florida: Chapman and Hall CRC) (https://doi.org/10.1175/JCLI3372.1)
[44] Livezey R E and Chen W Y 1983 *Mon. Weather Rev.* **111** 46–59
[45] Ropelewski C F and Halpert M S 1986 *Mon. Weather Rev.* **114** 2352–62
[46] Kahya E and Dracup J A 1993 *Water Resour. Res.* **29** 2491–503
[47] Bell G D and Halpert M S 1998 Climate Assessment for 1997 (https://doi.org/10.1175/1520-0477(1998)079<1014:CAF>2.0.CO;2)
[48] Cayan D R, Redmond K T and Riddle L G 1999 *J. Clim.* **12** 2881–93
[49] Dettinger M D, Cayan D R, Mccabe G J and Redmond K T 2000 *Exp. Long-Lead Forecast Bull.* **9** 55–60
[50] Redmond K T and Koch R W 1991 *Water Resour. Res.* **27** 2381–99
[51] Cayan D R and Peterson D H 1989 The influence of north pacific atmospheric circulation on streamflow in the west *Aspects of Climate Variability in the Pacific and the Western Americas* (Florida, NW: American Geophysical Union) pp 375–97

[52] Harshburger B, Ye H and Dzialoski J 2002 *J. Hydrol.* **264** 157–69

[53] Ropelewski C F and Halpert M S 1996 *J. Clim.* **9** 1043–59

[54] Herdies D L 2002 *J. Geophys. Res.* **107** 8075

[55] Eltahir E A B 1996 *Water Resour. Res.* **32** 131–137

[56] Zaroug M A H, Giorgi F, Coppola E, Abdo G M and Eltahir E A B 2014 *Hydrol. Earth Syst. Sci.* **18** 4311–23

[57] Abtew W, Melesse A M and Dessalegne T 2009 *Hydrol. Process.* **2274** 3653–60

[58] Mariotti A 2002 *Geophys. Res. Lett.* **29** 1621

[59] Brönnimann S 2007 *Rev. Geophys.* **45** 2006RG000199

[60] Shaman J 2014 *J. Clim.* **27** 6423–38

[61] Niedzielski T 2011 *Pure Appl. Geophys.* **168** 871–886

[62] Folland C K 2002 *Geophys. Res. Lett.* **29** 1643

[63] Zhang R, Li T, Wen M and Liu L 2015 *Clim. Dyn.* **45** 559–67

[64] Lu R Y, Hong X W and Li X Y 2016 *Atmos. Ocean. Sci. Lett.* **9** 185–90

[65] Chen J M, Li T and Shih C F 2008 *J. Meteorol. Soc. Jpn.* **86** 297–312

[66] Capotondi A *et al* 2015 *Bull. Am. Meteorol. Soc.* **96** 921–38

[67] Liang Y C, Chou C C, Yu J Y and Lo M H 2016 *Environ. Res. Lett.* **11** 044012

[68] Ward P, Jongman B, Kummu M, Dettinger M, Sperna Weiland F and Winsemius H 2014 *Proc. Natl Acad. Sci. USA* **111** 15659–64